Research Article

Aleksander Muc* and Małgorzata Muc-Wierzgoń

Effects of Material Constructions on Supersonic Flutter Characteristics for Composite Rectangular Plates Reinforced with Carbon Nano-structures

https://doi.org/10.1515/secm-2021-0010
Received Sep 29, 2020; accepted Jan 31, 2021

Abstract: In this paper effects of material constructions on natural frequencies and critical aerodynamic pressures are investigated. It is assumed that the rectangular plate is made of a polymeric matrix reinforced with graphene nanoplatelets or carbon nanotubes. A general closed analytical method of solution is presented. It is demonstrated that three parameters define entirely the location of the critical flutter pressure. The influence of material properties and transverse shear effects is characterized by a set of multipliers. They can be easily adopted in design procedures.

Keywords: Construction of material properties; Rectangular plates; Nanocomposites; Supersonic flutter; Nanoplatelets; Carbon nanotubes

1 Introduction

Observing the current trends in the advancement of manufacturing technologies and 3D-printing techniques one can notice that various materials can be created/formed with the desired in advance variation in of material properties along different directions of designed structures, such as *e.g.*:

- *Metamaterials* – materials with a programed design of the internal microstructure and extraordinary properties which have not been found in natural materials – see the examples presented in Refs [1–4]
- Since *FGMs* (Functionally Graded Materials) have some extraordinary properties, namely, a high temperature and a corrosion resistance, as well as an improved residual stress distribution, they are widely studied in many fields of the applied sciences and they are adopted as structural components in military, medical, or aerospace industries, as well as in power plants or vessels. Thus, due to their special privileges in comparison with traditional materials, most industries make effort to exert such materials in lieu of ordinary ones [5–8].
- *Porous FGM* – with the porosities produced during the fabrication process, the perfect FGM plate will become an imperfect FGM plate. The porosity model can be further classified as even and uneven porosity models according to the distribution characteristic of porosities Porosities inside materials can be distributed with many different types. They can be distributed uniform, non- uniform, or graded function. Basically, porosity reduces the stiffness of the structure,
- *Metal Foams* – the application of nanoporous metal foams (NPMFs) has been extended to some advanced engineering fields due to their extremely high specific surface area. The structural behaviour of constructions made of NPMF was studied by several researchers – see *e.g.* [9–13].
- *Nanocomposites* – the existence of pores in FGMs can lead to the loss of stiffness, density etc. To increase the loss of properties carbon nano-structures can be used as nano-fillers [14–16], *e.g.* carbon nano-tubes (CNTs) or graphene platelets (GPLs). The application of nanostructures was extensively investigated *e.g.* in Refs [17–24]. Recently the attention has been also focused on the possible application of 3D graphene foams (GrFs) [25–29]. The possible methods of the analysis of FGM plates reinforced by nanocomposites are discussed *e.g.* in Ref [30–33] and references therein.

The broader discussion of the above problems is presented by Muc *et al.* [34, 35]. It is necessary to mention that the demonstrated list of materials seems to be artificial and scatter. However, the differences between the material properties has no influence on the general methodology of the

***Corresponding Author: Aleksander Muc:** Institute of Machine Design, Cracow University of Technology, Kraków, Poland; Email: olekmuc@mech.pk.edu.pl
Małgorzata Muc-Wierzgoń: Dept. of Internal Medicine, Medical University of Silesia, Katowice, Poland

analysis of free vibrations or static (buckling) and dynamic properties for 2D structures (rectangular plates, shallow and cylindrical shells). This work belongs to a sequence of published by the author papers dealing with laminated structures [34–36] and porous FGMs [37].

The aim of the present paper is to investigate and compare the supersonic flutter behaviour of rectangular NPFMF plates reinforced with CNTs and GPLs. The analysis is conducted with the use of classical (CPT) and third order transverse shear deformation (HTSDT) theories. The fundamental relations are derived in an analytical way – see Muc, Flis [36]. We intend to propose simple formula that characterizes the effects of the plate constructions and transverse shear effects on critical aerodynamic pressures and natural frequencies. The introduction to the problems of optimal design of FG plates is presented in Ref [38] for structures modeled as beams (an infinite width plate).

2 Material Properties of Nanocomposites

Let consider the rectangular composite plate where the airflow is directed along the x axis – Figure 1. The plate is made of a polymer matrix reinforced with nanoplatelets or carbon nanotubes. The material properties are derived with the use of homogenization theories and are described below in this section and in the Appendix.

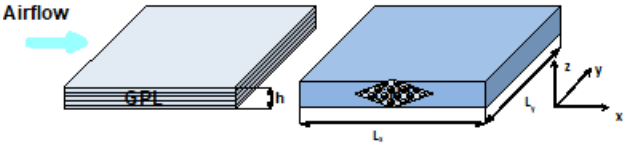

Figure 1: The geometry of the rectangular plate.

2.1 Graphene Nanoplatelets

The rectangular plate consists of N layers having the identical thickness $h^{(k)} = h/N$ but the porosity fraction and GPL fraction varies from layer to layer. Possible variants of the wall construction are demonstrated in Figure 2.

The effective, kth layer, material properties were derived with the use of the Mori-Tanaka method [39]. They take the following form:

$$E_c^{(k)} = \frac{E_m}{8}\left(3\frac{1+\xi_l\eta_l V_{GPL}^{(k)}}{1-\eta_l V_{GPL}^{(k)}} + 5\frac{1+\xi_w\eta_w V_{GPL}^{(k)}}{1-\eta_w V_{GPL}^{(k)}}\right), \tag{1}$$

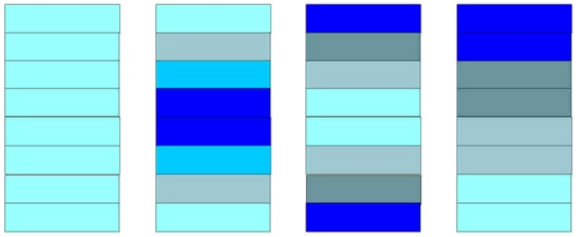

Figure 2: Variants of the wall constructions for plates reinforced with nanoplatelets: a) UD uniform distribution, b) FG – X symmetric distribution, c) FG – O symmetric distribution, d) FG – V unsymmetric distribution.

$$\eta_l = \frac{E_{GPL}-E_m}{E_{GPL}+\xi_l E_m}, \quad \eta_w = \frac{E_{GPL}-E_m}{E_{GPL}+\xi_w E_m}, \quad \xi_l = \frac{2l_{PGL}}{h_{PGL}}, \quad \xi_w = \frac{2w_{PGL}}{h_{PGL}}$$

where E_m denotes Young's modulus of the matrix, l_{GPL}, w_{GPL} and h_{GPL} are the average length, width and thickness of the GPLs, respectively. $V_{GPL}^{(k)}$ is the volume fraction of the kth layer:

$$V_{GPL}^{(k)} = \frac{g_{GPL}^{(k)}}{g_{GPL}^{(k)} + \left(\rho_{GPL}/\rho_m\right)\left(1-g_{GPL}^{(k)}\right)} \tag{2}$$

$g_{GPL}^{(k)}$ is the GPLs volume weight fraction. Four distributions of carbon nanoplatelets are considered:

$$g_{GPL}^{(k)} = 2g_{GPL}^{\star}\begin{cases} 1/2 & \text{UD} \\ \frac{N+1-|N+1-2k|}{N+2} & \text{FG - O} \\ \frac{1+|N+1-2k|}{N+2} & \text{FG - X} \\ \frac{k}{N+1} & \text{FG - V} \end{cases} \tag{3}$$

The effective nanocomposite density is characterized by the classical mixture law:

$$\rho_c^{(k)} = \rho_{GPL}V_{GPL}^{(k)} + \rho_m\left(1-V_{GPL}^{(k)}\right) \tag{4}$$

The symbol ρ denotes density of the kth layer ($\rho_c^{(k)}$), of the matrix (ρ_m) and of the GPLs (ρ_{GPL}).

The distributions of the graphene nano-plates are symmetric with respect to the plate mid-plane for configurations denoted as UD, FG-O, FG-X and antisymmetric for FG-V.

2.2 Carbon nanotubes

Now, considering the reinforcement of plates with CNTs the homogenized Young moduli can be derived from the

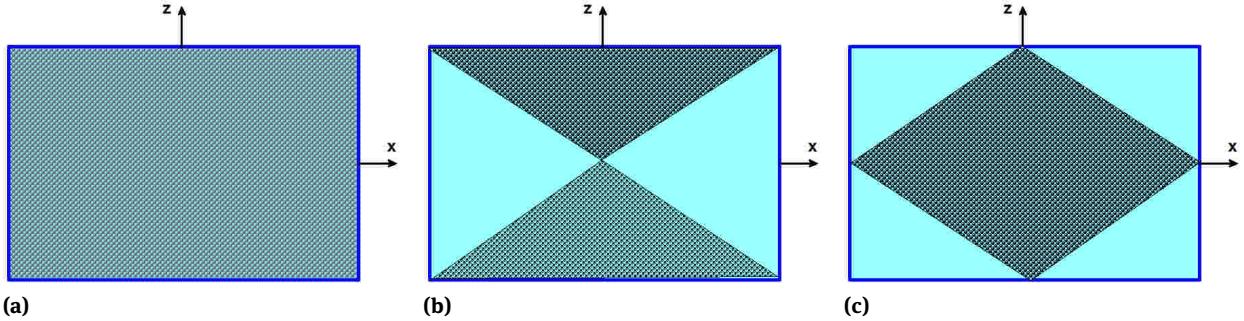

Figure 3: Configurations of cross-sections reinforced with carbon nanotubes: a) uniform distribution, b) symmetric distribution FG – X, c) symmetric distribution FG – O.

following relations [40]:

$$E_{11} = \eta_1 E_{11}^{CNT} V^{CNT}(z) + E_m V^m(z), \qquad (5)$$
$$\frac{\eta_2}{E_{22}} = \frac{V^{CNT}(z)}{E_{22}^{CNT}} + \frac{V^m(z)}{E_m}, \frac{\eta_3}{G_{12}} = \frac{V^{CNT}(z)}{G_{12}^{CNT}} + \frac{V^m(z)}{G_m}$$

where the volume fractions of the three distribution types of CNTs are characterized by the relations:

$$V^{CNT}(z) = V_\star^{CNT} \begin{cases} \frac{1}{1} & \text{UD} \\ 2\left(1 - \frac{2|z|}{h}\right) & \text{FG - O} \\ \frac{4|z|}{h} & \text{FG - X} \end{cases} \qquad (6)$$

$$V(z) = V^{CNT}(z)\rho_{CNT} + V_m(z)\rho_m \qquad (7)$$

3 Method of the solution

3.1 Governing relations

Various formulations of 2D kinematical relations can be applied to the description of plate deformations. A broad review of them is presented in Refs [41, 42]. In the present work the third order transverse shear deformation theory (TTSDT) is used where 3D linear components of displacements can be expressed in the following way:

$$U_1(x,y,z) = u(x,y) + z\psi_1(x,y) - cz^3\left[\psi_1(x,y) + \frac{\partial w(x,y)}{\partial x}\right] \qquad (8)$$
$$U_2(x,y,z) = v(x,y) + z\psi_2(x,y) - cz^3\left[\psi_2(x,y) + \frac{\partial w(x,y)}{\partial y}\right]$$
$$U_3(x,y,z) = w(x,y)$$

where u, v, w, ψ_1, ψ_2 describe the unknown functions defining the deformations of any point at the plate mid-surface, and c is a constant. Prescribing $c = 0$ the above relations are valid for the first order transverse shear deformation theory (FSDT). Further simplification can be obtained by the assumptions:

$$\psi_1(x,y) = -\frac{\partial w(x,y)}{\partial x}, \quad \psi_2(x,y) = -\frac{\partial w(x,y)}{\partial y} \qquad (9)$$

The number of unknowns is reduced to three u, v, w and such a formulation is called as the classical plate theory (CPT).

In the case of TTSDT the set of equilibrium equations is reduced to the following form:

$$\frac{\partial N_{xx}}{\partial x} + \frac{\partial N_{xy}}{\partial y} = 0, \quad \frac{\partial N_{xy}}{\partial x} + \frac{\partial N_{yy}}{\partial y} = 0 \qquad (10)$$
$$\frac{\partial Q_{xz}}{\partial x} + \frac{\partial Q_{yz}}{\partial y} - 3c\left(\frac{\partial R_{xz}}{\partial x} + \frac{\partial R_{yz}}{\partial y}\right) + c\left(\frac{\partial^2 P_{xx}}{\partial x^2} + 2\frac{\partial^2 P_{xy}}{\partial x \partial y} + \frac{\partial^2 P_{yy}}{\partial y^2}\right) = \hat{\rho}\frac{\partial^2 w}{\partial \tau^2} - \lambda\frac{\partial w}{\partial x}$$
$$\frac{\partial M_{xx}}{\partial x} + \frac{\partial M_{xy}}{\partial y} - Q_{xz} + 3cR_{xz} - c\left(\frac{\partial P_{xx}}{\partial x} + \frac{\partial P_{xy}}{\partial y}\right) = 0,$$
$$\frac{\partial M_{xy}}{\partial x} + \frac{\partial M_{yy}}{\partial y} - Q_{yz} + 3cR_{yz} - c\left(\frac{\partial P_{xy}}{\partial x} + \frac{\partial P_{yy}}{\partial y}\right) = 0$$

$$\begin{Bmatrix} N \\ M \\ P \end{Bmatrix} = \begin{bmatrix} A & B & C \\ B & D & F \\ C & F & G \end{bmatrix} \begin{Bmatrix} \varepsilon^{(0)} \\ \varepsilon^{(1)} \\ \varepsilon^{(3)} \end{Bmatrix} \qquad (11)$$

$$\begin{Bmatrix} \varepsilon_{xx} \\ \varepsilon_{yy} \\ \varepsilon_{xy} \end{Bmatrix} = \begin{Bmatrix} \varepsilon_{xx}^{(0)} \\ \varepsilon_{yy}^{(0)} \\ \varepsilon_{xy}^{(0)} \end{Bmatrix} + z\begin{Bmatrix} \varepsilon_{xx}^{(1)} \\ \varepsilon_{yy}^{(1)} \\ \varepsilon_{xy}^{(1)} \end{Bmatrix} + z^3\begin{Bmatrix} \varepsilon_{xx}^{(3)} \\ \varepsilon_{yy}^{(3)} \\ \varepsilon_{xy}^{(3)} \end{Bmatrix} \qquad (12)$$

$N(M.P)$ denotes the vectors having three components (N_{xx}, N_{yy}, N_{xy}), whereas $Q(R)$ has two components only (Q_{xz}, Q_{yz}).

$$(A, B, C, D, F, G) = \int_{-h/2}^{h/2} \left(1, z, z^2, z^3, z^4, z^6\right)[Q]dz, \qquad (13)$$

$$i, j = 1, 2, 3$$

$$(H, I, J) = \int_{-h/2}^{h/2} \left(1, z^2, z^4\right) [Q] dz, \quad i, j = 4, 5$$

$[Q]$ is the reduced stiffness constants of materials defined as follows:

$$[Q] = \begin{bmatrix} E_{11}/(1-\nu_{12}\nu_{21}) & \nu_{21}E_{11}/(1-\nu_{12}\nu_{21}) & 0 & 0 & 0 \\ \nu_{21}E_{11}/(1-\nu_{12}\nu_{21}) & E_{21}/(1-\nu_{12}\nu_{21}) & 0 & 0 & 0 \\ 0 & 0 & G_{12} & 0 & 0 \\ 0 & 0 & 0 & G_{23} & 0 \\ 0 & 0 & 0 & 0 & G_{13} \end{bmatrix}, \tag{14}$$

$$\nu_{21}E_{11} = \nu_{12}E_{22}$$

3.2 Two parallel simply supported edges

For two simply supported parallel opposite edges the general form of the solution can be searched in the following way:

$$u(x, y) = \sum_{n=1}^{\infty}\sum_{m=1}^{4} U_{mn} \exp\left(\alpha_m x/L_x\right) \sin\left(\delta_n y\right) \tag{15}$$

$$v(x, y) = \sum_{n=1}^{\infty}\sum_{m=1}^{4} V_{mn} \exp\left(\alpha_m x/L_x\right) \cos\left(\delta_n y\right)$$

$$w(x, y) = \sum_{n=1}^{\infty}\sum_{m=1}^{4} W_{mn} \exp\left(\alpha_m x/L_x\right) \sin\left(\delta_n y\right)$$

$$\psi_1(x, y) = \sum_{n=1}^{\infty}\sum_{m=1}^{4} \Theta_{xmn} \exp\left(\alpha_m x/L_x\right) \sin\left(\delta_n y\right)$$

$$\psi_2(x, y) = \sum_{n=1}^{\infty}\sum_{m=1}^{4} \Theta_{xmn} \exp\left(\alpha_m x/L_x\right) \cos\left(\delta_n y\right)$$

$$\delta_n = \frac{\pi n}{L_y}, n = 1, 2, \ldots.$$

Inserting the relations (15) in the equilibrium equations (10) one can obtain the system of five algebraic equations. For CPT it is reduced to one characteristic equation:

$$\left(\alpha_m^2 - \pi^2 k\right)^2 + \beta^* \alpha_m - \lambda^* = 0 \tag{16}$$

The analytical solution of the above characteristic equation exists and it is discussed in Ref [32]. It may be represented as the function of two variables ς and υ and takes the following form:

$$\alpha_{1,2} = \varsigma \pm i\upsilon, \tag{17}$$

$$\alpha_{3,4} = -\varsigma \pm \sqrt{2k\pi^2 + \upsilon^2 - 2\varsigma^2}, \quad i = \sqrt{-1}$$

and the coefficients β^* and λ^* are expressed as follows:

$$\beta^* = 4\varsigma\left(\upsilon^2 - \varsigma^2 + k\pi^2\right), \tag{18}$$

$$\lambda^* = k^2\pi^4 + \left(\upsilon^2 + \varsigma^2\right)\left(\upsilon^2 - 3\varsigma^2 + 2k\pi^2\right)$$

The explicit form of the determinant (called as the eigencurve) characterizing the influence of the boundary conditions along the edges $x = 0$ and $x = L_x$ is also the function of two variables ς and υ. For instance for the plates with the prescribed simply-supported boundary conditions it takes the following form:

$$\Delta(\varsigma, \upsilon, k) = \cosh(2\varsigma) - \cos(\upsilon)\cosh\sqrt{2k\pi^2 + \upsilon^2 - 2\varsigma^2} + \left[k^2\pi^4 + 3\varsigma^4 - 2\varsigma^2\upsilon^2 + \upsilon^4 + 2k\pi^2\left(-2\varsigma^2 + \upsilon^2\right)\right] x \frac{\sin(\upsilon)\sinh\sqrt{2k\pi^2 + \upsilon^2 - 2\varsigma^2}}{2\varsigma^2\upsilon\sqrt{2k\pi^2 + \upsilon^2 - 2\varsigma^2}} \tag{19}$$

In the plane ς and υ it is possible to plot the determinant and the parameters λ^* (proportional to the eigenfrequency) and β^* (proportional to the aerodynamic pressure) – see Figure 4. The critical point corresponding to the flutter phenomena is described as the single point arising as the tangent between the trajectories of the determinat and of the curve β^*_{crit}. The value of the critical aerrodynamic pressure is defined by the value λ^*_{crit} cutting the critical point. To identify the influence of the material distribution on the value of the critical aerodynamic pressures it is necessary to analyse the inluence of three parameters k, λ^* and β^* on the position of the critical point drawn in Figure 4.

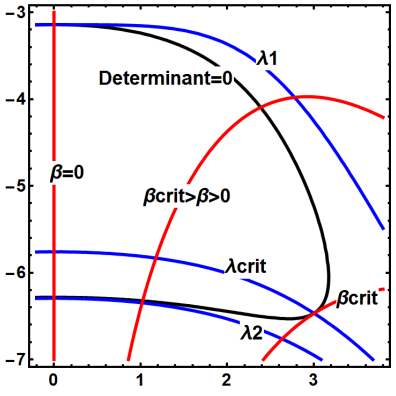

Figure 4: Evaluation of natural neighbourhood frequencies and critical (flutter) pressure (simply supported edges).

The effects of the parameter k can be easily derived plotting the values of the determinant (19) – Figure 5. The locations of the critical points are shifted as the value of k increases.

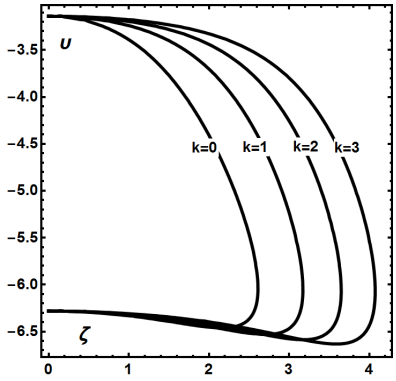

Figure 5: The influence of the parameter k on the distribution of eigencurves for rectangular plates with simply supported edges.

4 Numerical results

4.1 Classical plate theory

At the beginning the research of the material distribution effects on the flutter characteristics is carried out for moderately thin plates ($h/L_x = 0.05$) employing the classical plate equations. Various material distributions of graphene nanoplatelets and carbon nanotubes reinforcement are compared to the isotropic material.

Isotropic structures

The definition of three parameters controlling the flutter behaviour is presented below:

$$k = \left(\frac{nL_x}{L_y}\right)^2, \quad \beta^\star = \frac{\Lambda L_x^3}{D^{isotr}}, \tag{20}$$

$$\lambda^\star = \rho h \omega^2 \frac{L_x^4}{D^{isotr}}, \quad D^{isotr} = \frac{Eh^3}{12\left(1-\nu^2\right)}$$

Let us note that for plates with an infinite width ($L_y \to \infty$) k is equal to zero, and for the square plates and n=1 k is equal to 1. The values of the $\lambda^\star$ and $\beta^\star$ parameters are the functions of the bending stiffness D^{isotr}.

Graphene Platelets – isotropic

Although graphene platelets possess the isotropic properties the definition of the controlling parameters $\lambda^\star$ and $\beta^\star$ is changed (Eq. (21)) due to nonhomogeneous distributions of material distributions. Figures 6a and 6b demonstrate the distributions of Young's moduli derived for various configurations of the reinforcement – Eq. (3). The material constants of the graphene platelets composites considered herein are following (Ref [39]): $GPL - E_{GPL} = 1.01$ TPa, $\nu_{GPL} = 0.186$, $l_{GPL} = 2.5\mu$m, $w_{GPL} = 1.5\mu$m, $h_{GPL} = 1.5$ nm, $g^\star_{GPL} =$ 1%, $\rho_{GPL} = 1060$ kg/m^3, Matrix - $E_m = 3.0$GPa, $\nu_m = 0.34$, $\rho_m = 1200$ kg/m^3.

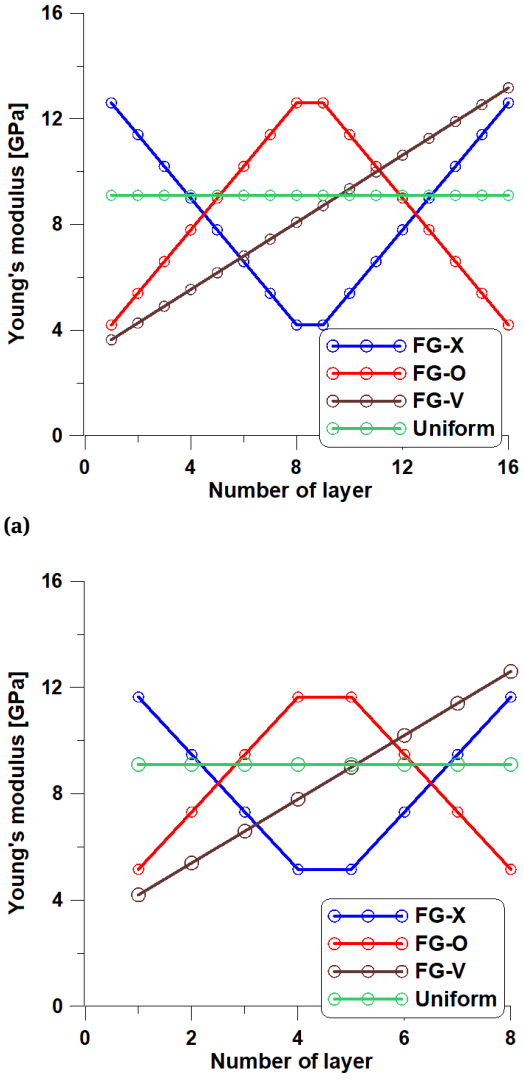

Figure 6: Distributions of the Young modulus for different configuration of the nanoplatelets reinforcement and the polymer matrix: a) N=16, b) N=8.

In addition for unsymmetric configuration (FG-V) the coupling matrix [B] is not equal to zero.

$$k = \left(\frac{nL_x}{L_y}\right)^2, \quad \beta^\star = \Lambda L_x^3 M, \quad \lambda^\star = \omega^2 \hat{M} L_x^4, \tag{21}$$

$$M = \frac{A}{-B^2 + AD}, \quad \hat{M} = \hat{\rho} M, \quad A = \int_{-h/2}^{h/2} Q_{11}(z)dz,$$

$$B = \int_{-h/2}^{h/2} Q_{11}(z) z dz, \quad D = \int_{-h/2}^{h/2} Q_{11}(z) z^2 dz,$$

$$\hat{\rho} = \int_{-h/2}^{h/2} \rho(z)dz, \quad Q_{11}(z) = \frac{E(z)}{1-\nu^2}$$

To illustrate the effects of reinforcement configuration let us compare the values of λ^* and β^* with let us write the following equalities:

$$\beta_{crit}^{*(ref)} = \frac{\Lambda L_x^3}{D^{(ref)}} = \beta_{crit}^* = \Lambda L_x^3 M \tag{22}$$

$$\text{then} \quad \beta_{crit}^* = \frac{1}{D^{(ref)}M}$$

$$\lambda_{crit}^{*(ref)} = \frac{\omega^{2(ref)}\rho^{(ref)}L_x^4}{D^{(ref)}} = \lambda_{crit}^* = \omega^2 \hat{M} L_x^4$$

$$\text{then} \quad \omega^2 = \frac{\omega^{2(ref)}\rho^{(ref)}}{\hat{M}D^{(ref)}}$$

Assuming that the reference eigencurve is evaluated for the matrix properties it can be found easily that for uniform distributions of platelets:

$$\beta_{crit}^* = \beta_{crit}^{*(m)} \frac{E^{UD}}{E^m} \tag{23}$$

The above values increasecomparing to thematrix. The degree of the growthis a function of the multipliers M, $\hat{M}$ and in this way of the material configuration of the nanoplatelets reinforcement. The examples of the flutter characteristics are illustrated in Figure 7. For a simply-supported square plate of dimension L_x the natural frequencies can be derived from the relation: $\omega^2 = \pi^4 D^{(ref)}\left(m^2+n^2\right)^2 / \left(L_x^4 \rho^{(ref)} h\right)$ so that the multiplier $\pi^4(m^2+n^2)^2$ is equal to 389.64 (m=n=1) and to 2435.23 (m=2, n=1) – see Figure 7, where the prescribed reference value is identical to the matrix properties. In Ref [31] (Figure 8) the dimensionless critical pressure (related to the matrix properties) is equal to 512.5 plotted in Figure 7. Evaluating the dimensionless flutter characteristics for square plates reinforced with UD graphene nanoplates one can observe the increase of the flutter pressures and of the natural frequencies. Let us note that the growth of the mentioned above values is in a very good agreement with the analytical predictions Eq. (23) and the data plotted in Figure 6 for isotropic uniformly distributed reinforcement (the ratio E^{UD}/E^m is equal to 3 – the Appendix).

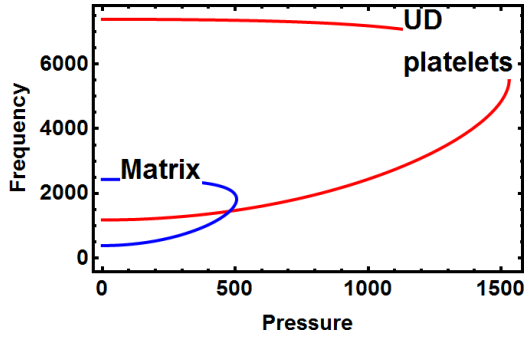

Figure 7: The change of the dimensionless flutter characteristics for simply supported square plates.

Carbon nanotubes – anisotropic (symmetric configuration $E(z) = E(-z)$)

Composites reinforced by carbon nanotubes have the following material properties (Ref. [40]): CNT – $E_{11}^{CNT} = 5.6466$ TPa, $E_{22}^{CNT} = 7.0800$ TPa, $G_{12}^{CNT} = 1.9455$ TPa, $\nu^{CNT} = 0.175$, $\rho^{CNT} = 1400$ kg/m^3, $\eta_1 = 0.137$, $\eta_2 = 1.022$, $\eta_3 = 0.715$, $V_\star^{CNT} = 0.12$; Matrix – $E_m = 3.52$ GPa, $\nu_m = 0.34$, $\rho_m = 1150$ kg/m^3.

For carbon nanotube reinforcement the controlling parameters are defined by the relation (24).

$$k = \frac{D_{12}+2D_{33}}{D_{11}}\left(\frac{nL_x}{L_y}\right)^2, \quad \beta^* = \frac{\Lambda L_x^3}{D_{11}}, \tag{24}$$

$$\lambda^* = \hat{\rho}\omega^2 \frac{L_x^4}{D_{11}} - \frac{D_{22}}{D_{11}}\left(\frac{n\pi L_x}{L_y}\right)^4 - 4\pi^4 k^2$$

$$D_{ij} = \int_{-h/2}^{h/2} Q_{ij}(z)z^2 dz, \; i,j = 1,2,3$$

For the analysed mechanical properties of the nanocomposite (the Appendix) the multiplier is equal 0.01 and assuming that the wavenumber n is equal to1 and $L_x = L_y$ the value of the k parameter is almost equal to zero. However, Zhang *et al.* [17] reported that the lowest wavenumber n is equal to 13 what results in a drastic increase of the coefficient k – Figure 8.

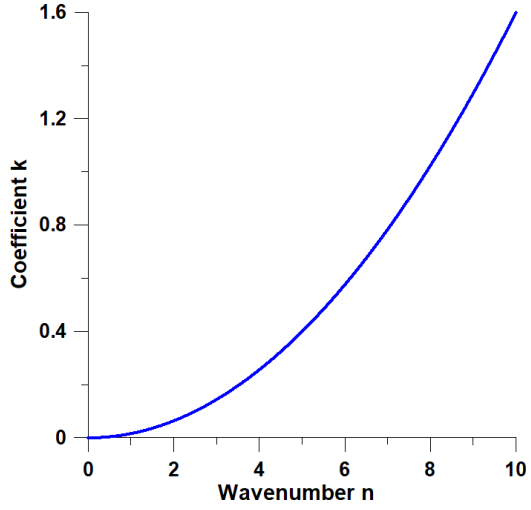

Figure 8: Variations of the coefficient k with wavenumber n.

Considering the values of the parameter λ^* the increase of the critical aerodynamic pressure is a proportional, linear function of the bending stiffnesses D_{11}. Therefore the relation between the configurations of nanotubes reinforcement (6) is directly determined by the inequalities: $D_{11}^{FG-X} = E_1h^3/[8(1-\nu_{12}\nu_{21})] > D_{11}^{UD} = E_1h^3/[12(1-\nu_{12}\nu_{21})] > D_{11}^{FG-O} = E_1h^3/[24(1-\nu_{12}\nu_{21})]$. Anisotropic reinforcement reduces the values of natural frequencies – the parameter β^*.

4.2 Transverse shear effects

The derivation of the characteristic equation for transverse shear theory is much more complicated as it is shown in Ref [35], particularly due to the complexity of the relations (8)–(14). Therefore, it is much better to implement numerical approximations and the Rayleigh-Ritz method – see *e.g.* Ref. [43]. Figure 9 demonstrates the characteristic features of the use of transverse shear deformation theories, *i.e.*:

- The decrease of the natural frequencies
- The growth of the critical aerodynamic pressures

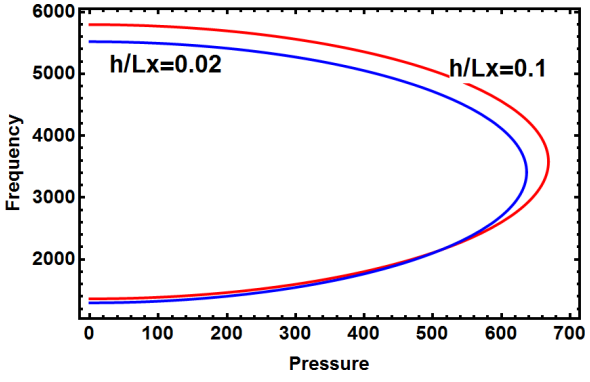

Figure 9: Transverse shear deformation effects – square fully clamped plates.

The results are presented in the dimensionless form and referred to the value $\omega^{(ref)2} = D^{(ref)}/\left(L_x^4\rho^{(ref)}h\right)$ for natural frequencies and to $\Lambda L_x^3/D^{(ref)}$ for aerodynamic pressure. Using CPT Leissa [44] computed two first eigenfrequencies and he obtained the following dimensionless quantities $\omega_{11}^2 = 1295.78$ and $\omega_{21}^2 = 5389.47$. As it may be seen the agreement between the predicted natural frequencies plotted in Figure 9 and presented in the literature is quite good.

5 Conclusions

Aeroelastic behavior of polymeric rectangular plates reinforced with graphene nanoplatelets or carbon nanotubes is studied in this paper. For the material properties (stiffness and density), different groups of material distributions are investigated.

Based on the analytical studies and simulation results conducted with the use of the Mathematica package, the following conclusions can be drawn:

1. It is proved that three parameters can control entirely the appearance of the flutter phenomena, *i.e.* the coalescence of vibration modes;
2. Using the relations valid for CPT the influence of the above parameters can be evaluated in an analytical way as two parallel edges are simply supported;
3. Both for GPLs and CNTs reinforcement the value of the bending stiffness along the airflow direction seems to be the most significant parameter affecting on the value of the critical aerodynamic pressure; the growth of the bending stiffness results in the increase of the aerodynamic pressure similarly as for laminated multilayered plates;
4. The effects of unsymmetric with respect to the midplane should can be taken into account by the introduction of two multipliers characterizing the coupling effects between bending and membrane states of deformations; it should be pointed out that membrane deformations lead to the complication of fundamental governing relations;
5. The analysis of transverse shear effects can be carried out with the use of numerical procedures implementing the Rayleigh-Ritz method; it is observed that transverse shear deformation effects reduce the values of natural frequencies and increase simultaneously the values of critical pressures comparing to the results evaluated with the use of classical plate theory.

The mentioned above conclusions (1)–(5) determine precisely and entirely the contribution of the author to the problems of free vibrations and flutter characteristics evaluation for rectangular plates reinforced with graphene nanoplatelets or carbon nanototubes. The identical procedures can be easily adopted to the analysis of aerothermoelastic effects and of sandwich structures with fibre reinforced plastics faces.

References

[1] Yu, X.; Zhou, J.; Liang, H.; Jiang, Z.; Wu, L. Mechanical metamaterials associated with stiffness, rigidity and compressibility: A brief review. Prog. Mater. Sci. **2018**, 94, 114–173.

[2] Ren, C.; Yang, D.; Qin, H. Mechanical performance of multidirectional buckling-based negative stiffness metamaterials: An analytical and numerical study. Materials. **2018**, 11, 1078.

[3] Zadpoor, A.A. Mechanical meta-materials. Mater. Horiz. **2016**, 3, 371–381.

[4] S. Gao, W. Liu, L. Zhang, Asit Kumar Gain. A New Polymer-Based Mechanical Metamaterial with Tailorable Large Negative Poisson's Ratios. Polymers 2020, 12, 1492;

[5] Birman, V.; Byrd, L.W. Modeling and analysis of functionally graded materials and structures. Appl. Mech. Rev. **2007**, 60, 195–216.

[6] Miyamoto, Y.; Kaysser, W.A.; Rabin, B.H.; Kawasaki, A.; Ford, R.G. Functionally Graded Materials: Design, Processing and Applications; Springer Science & Business Medi: New York, NY, USA, 2013.

[7] Noda, N. Thermal stresses in functionally graded materials. J. Therm. Stress. **1999**, 22, 477–512.

[8] Shen, H.S. Functionally Graded Materials: Nonlinear Analysis of Plates and Shells; CRC Press: Boca Raton, FL, USA, 2016.

[9] Pollien A, Conde Y, Pambaguian L, Mortensen A. Graded open-cell aluminium foam core sandwich beams. Mater Sci Eng, A 2005;404:9–18.

[10] Pia, G.; Delogu, F. On the elastic deformation behavior of nanoporous metal foams. Scr. Mater. **2013**, 69, 781–784.

[11] Park, H.; Ahn, C.; Jo, H.; Choi, M.; Kim, D.S.; Kim, D.K.; Jeon, S.; Choe, H. Large-area metal foams with highly ordered submicrometer-scale pores for potential applications in energy areas. Mater. Lett. **2014**, 129, 174–177.

[12] Heydari, H.; Moosavifard, S.E.; Shahraki, M.; Elyasi, S. Facile synthesis of nanoporous CuS nanospheres for high-performance supercapacitor electrodes. J. Energy Chem. **2017**, 26, 762–767.

[13] Li, J.; Wang, S.; Xiao, T.; Tan, X.; Xiang, P.; Jiang, L.; Deng, C.; Li, W.; Li, M. Controllable preparation of nanoporous Ni3S2 films by sulfuration of nickel foam as promising asymmetric supercapacitor electrodes. Appl. Surf. Sci. **2017**, 420, 919–926.

[14] Esawi AM, Farag MM. Carbon nanotube reinforced composites: Potential and current challenges. Mater Des 2007;28:2394–401.

[15] Liew K, Lei Z, Zhang L. Mechanical analysis of functionally graded carbon nanotube reinforced composites: A review. Compos Struct 2015;120:90–7.

[16] Kim H, Abdala AA, Macosko CW. Graphene/polymer nanocomposites. Macromolecules 2010;43:6515–30.

[17] Zhang LW, Song ZG, Liew KM, Computation of aerothermoelastic properties and active flutter control of CNT reinforced functionally graded composite panels in supersonic airflow, Comput. Methods Appl. Mech. Engrg. 300 (2016) 427–441.

[18] Zhang Y, Zhang F, Vibration and Buckling of Shear Deformable Functionally Graded Nanoporous Metal Foam Nanoshells, Nanomaterials **2019**, 9, 271;

[19] Aditya S, Haboussi M, Shubhendu S, Ganapathi M. Polit O, Supersonic flutter study of porous 2D curved panels reinforced with graphene platelets using an accurate shear deformable finite element , procedure, Composite Structures 241 (2020) 112058

[20] Barati, M.R.; Zenkour, A.M. Investigating post-buckling of geometrically imperfect metal foam nanobeams with symmetric and asymmetric porosity distributions. Compos. Struct. **2017**, 182, 91–98.

[21] Sahmani, S.; Aghdam, M.M.; Rabczuk, T. Nonlinear bending of functionally graded porous micro/nano-beams reinforced with graphene platelets based upon nonlocal strain gradient theory. Compos. Struct. **2018**, 186, 68–78.

[22] Wang, Y.Q.; Zhao, H.L.; Ye, C.; Zu, J.W. A Porous Microbeam Model for Bending and Vibration Analysis Based on the Sinusoidal Beam Theory and Modified Strain Gradient Theory. Int. J. Appl. Mech. **2018**, 10, 1850059.

[23] Huang K, Guo H, Qin Z, Cao S., Chen Y, Flutter analysis of laminated composite quadrilateral plates reinforced with graphene nanoplatelets using the element-free IMLS-Ritz method, Aerospace Science and Technology 103 (2020) 105915

[24] Muc, A., Modelling of carbon nanotubes behaviour with the use of a thin shell theory, J. Th. Appl Mech, 2011, 49 (2), pp. 531-540.

[25] Li, N.; Zhang, Q.; Gao, S.; Song, Q.; Huang, R.; Wang, L.; Liu, L.; Dai, J.; Tang, M.; Cheng, G. Three-dimensional graphene foam as a biocompatible and conductive scaffold for neural stem cells. Sci. Rep. **2013**, 3, 1604.

[26] Wu, Y.; Yi, N.; Huang, L.; Zhang, T.; Fang, S.; Chang, H.; Li, N.; Oh, J.; Lee, J.A.; Kozlov, M. Three-dimensionally bonded spongy graphene material with super compressive elasticity and near-zero Poisson's ratio. Nat. Commun. **2015**, 6, 6141.

[27] Qin, Z.; Jung, G.S.; Kang, M.J.; Buehler, M.J. The mechanics and design of a lightweight three-dimensional graphene assembly. Sci. Adv. **2017**, 3, 1–9.

[28] Huang, X.; Qian, K.; Yang, J.; Zhang, J.; Li, L.; Yu, C.; Zhao, D. Functional nanoporous graphene foams with controlled pore sizes. Adv. Mater. **2012**, 24, 4419–4423.

[29] Y. Liu, Y. Wang, Size-Dependent Free Vibration and Buckling of Three-Dimensional Graphene Foam Microshells Based on Modified Couple Stress Theory, Materials **2019**, 12, 729

[30] Noroozi, A. R., Malekzadeh P. Dimitri R., Tornabene F., Meshfree Radial Point Interpolation Method for the Vibration and Buckling Analysis of FG-GPLRC Perforated Plates under an In-Plane Loading , 2020, Engineering Structures 221(111000):1-20

[31] Nematollahi M.S., Mohammadi H., Dimitri R., Tornabene F., Nonlinear vibration of functionally graded graphene nanoplatelets polymer nanocomposite sandwich beams, 2020, Appl.Sc., 10 (16), 5669

[32] Ghasemia A.R., Mohandesa M., Dimitri R., Tornabene F., Agglomeration effects on the vibrations of CNTs/fiber/polymer/metal hybrid laminates cylindrical shell, Composites Part B: Engineering, 167, 2019, pp. 700-716

[33] Jouneghani F. Z., Dimitri R., Bacciocchi M., Tornabene F., Free Vibration Analysis of Functionally Graded Porous Doubly-Curved Shells Based on the First-Order Shear Deformation Theory, Appl. Sci. 2017, 7(12), 1252

[34] Muc, A., Flis, J., Augustyn M., Optimal Design of Plated/Shell Structures under Flutter Constraints. A Literature Review, Materials, 2019, 12 (24), 4215.

[35] Muc A., Flis, J. Closed form solutions – Analysis and optimal design of supersonic composite laminated flat plates considering mechanical and thermal effects (2019) Composite Structures, 230, art. no. 111491

[36] Muc A, Flis J, Free Vibrations and Flutter Characteristics of Multilayered Laminated Cylindrical Panels, (2020) Composite Struct.

246, art. no. 112400.
[37] Muc A, Flis J, Flutter Characteristics and Free Vibrations of Rectangular Functionally Graded Porous Plates, Composite Structures, 2020, art. no. 113301 (in press).
[38] Muc, A, Optimizing the thickness/Stiffness Distribution of an Infinitely Wide Porous FGM Plates subjected to Supersonic Flutter Constraints, Mechanics of Composite Materials, 2021, 56 (6), pp.713-720.
[39] M.T. Song, J. Yang, S. Kitipornchai, et al., Buckling and post-buckling of biaxially compressed functionally graded multilayer graphene nanoplatelet-reinforced polymer composite plates, Int. J. Mech. Sci. 131 (2017) 345–355.
[40] Z.X. Lei, L.W. Zhang, K.M. Liew, Free vibration analysis of laminated FG-CNT reinforced composite rectangular plates using the kp-Ritz method, Compos. Struct. 127 (2015) 245–259.
[41] Pagani A., Valvano S., Carrera E., Analysis of laminated composites and sandwich structures by variable-kinematic MITC9 plate elements, J. Sandw. Str, and Mater, 2018, 20, pp.4-44.
[42] E. Carrera, S. Valvano, M. Filippi, Classical, higher-order, zig-zag and variable kinematic shell elements for the analysis of composite multilayered structures, European Journal of Mechanics - A/Solids Volume 72, November–December 2018, Pages 97-110
[43] Muc A., Transverse Shear Effects in Supersonic Flutter Problems for Composite Multilayered Rectangular Plates – Benchmark for Numerical Analysis, Composites Part C: Open Access, 2020, 1, art. no. 100001.
[44] Leissa AW, Free vibrations of rectangular plates, Journal of Sound and Vibration, 1973, 31(3), pp. 257-293